Collisional redistribution of light: Far-wing line shapes and polarizations for the Ba-(Ar,Xe) systems

W. J. Alford, N. Andersen,* K. Burnett,† and J. Cooper
Department of Physics, University of Colorado, Boulder, Colorado 80309
and Joint Institute for Laboratory Astrophysics, University of Colorado and National Bureau of Standards, Boulder, Colorado 80309
(Received 5 April 1984)

We have measured the far-wing collisional redistribution line shape, the redistributed fluorescence polarization, and the collisional alignment decay rates for barium perturbed by argon and xenon. The experiment was performed with a heated gas cell ($T\sim900$ K) with perturber-gas densities in the 1—30-Torr range and laser light detuned ±3—1000 cm^{-1} from the 5535-Å Ba I 6^1S-6^1P resonance line. Metal-vapor densities were determined by a Rayleigh scattering technique, which is outlined in detail. By correlating structure in the line shape with that of the polarization, we are able to make definitive statements about the interatomic potentials. The Ba data show strong similarities with previous experimental results for similar two-electron atoms, namely Ca, Sr, and Hg, and so our conclusions are of relevance to these systems as well.

I. INTRODUCTION

The fields of line broadening and collisional redistribution are interesting and presently very active areas of atomic physics. Line broadening has long been of interest to astrophysicists and plasma physicists as a means of determining conditions in harsh or remote environments. Historically redistribution has been important because of its role in the transport of radiation through various media, such as stellar atmospheres. Interest in line broadening and particularly redistribution has grown in the last 20 years because of advancing computer and laser technology. Computers have immensely increased the computational power of theorists, enabling them to make quantitative predictions for modern experiments. Lasers have provided an intense monochromatic source of light with well-defined polarization which makes sensitive redistribution experiments possible. We have performed such a redistribution experiment which requires elements of line broadening and redistribution theory for the interpretation. Combining results and methods from line broadening and redistribution has the advantage of providing information about both adiabatic interactions and the dynamical behavior of systems.

Collision-broadening experiments are capable of yielding information about the adiabatic interaction of one atom with another.[1,2] This is because collision-broadening experiments are concerned with the probability of absorption (or emission) of a photon during a collision. A typical redistribution scattering experiment, on the other hand, is illustrated in Fig. 1(a). In this experiment a photon of frequency ω_L and linear polarization $\hat{\epsilon}_L$ is incident on an atom undergoing collisions with nearby perturbers. The emitted-light spectrum [Fig. 1(b)] is observed at 90° to the incident-light direction. If ω_L is near a resonant frequency ω_0 of the atom, then the scattered-light spectrum (for weak incident fields) consists of a Rayleigh peak centered at the incident-light frequency and a fluorescence peak centered near the resonance transition. In addition to observing the emitted intensities, though, one may monitor the polarization [Fig. 1(c)] of the emitted light. The polarization P is defined as

$$P=\frac{I_{\parallel}-I_{\perp}}{I_{\parallel}+I_{\perp}},$$

where $I_{\parallel}$ and $I_{\perp}$ refer to the intensities of the scattered light polarized parallel and perpendicular to the incident-light polarization direction. For a $J=0$ to $J=1$ transi-

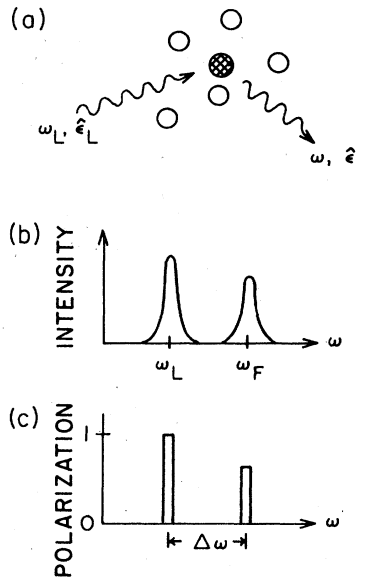

FIG. 1. (a) Light of frequency ω_L and polarization $\hat{\epsilon}_L$ is scattered off an atom surrounded by perturbers. (b) shows the intensity and (c) the polarization redistribution spectra of the scattered light [(c) assumes scattering off a ^1S ground state].

tion the Rayleigh scattering is completely polarized. The fluorescence peak is generally not completely polarized and may have a polarization of zero. The polarization of the fluorescence is determined largely by the dynamics of the collision and may yield information not available from line-broadening experiments.[3,4]

The first redistribution experiments were carried out by Carlsten *et al.*[5] for the Sr-Ar system at moderately high laser field strengths. Effects of high field strengths on the spectrum and dynamics of redistribution have been studied theoretically[6] and experimentally.[7] Redistribution theory for the impact region of the line profile and for weak field strengths was developed by Omont *et al.*[8] and Huber.[9] Theories applicable to the entire line shape which include effects of degeneracy have been developed by Burnett *et al.*[10–12] and Nienhuis.[13] Weak-field redistribution experiments have been performed on Ca-Ar by Corney and McGinley[14] in which the detuning dependence of the Rayleigh and fluorescence peaks was observed. The first redistribution scattering experiments with polarization analysis were done by Thomann *et al.*[15] for Sr-Ar and later extended to Sr perturbed by He, Ne, Kr, and Xe by Alford *et al.*[16] The present work describes a redistribution scattering experiment in which both the polarization and intensity of the fluorescence peak is monitored for barium being perturbed by argon and xenon.

This paper is divided into three major sections. Section II discusses pertinent features of collision-broadening theory and redistribution theory. This section emphasizes physical pictures of the relevant processes while making no attempt at mathematical rigor. Section III describes the experiment and presents the results. Included in this section is a description of our method for measuring vapor densities using Rayleigh scattering. Section IV contains the analysis of our results. In particular, based on our analysis and comparisons with similar systems, we discuss the qualitative behavior of the ground- and excited-state interatomic potentials.

II. THEORY

A. Line broadening and redistribution

Line broadening, in general, encompasses natural broadening, Doppler broadening, and collision broadening (with possible correlations between them). Natural and Doppler broadening (ignoring correlations with collision broadening) are well understood processes and are of no interest in this section. We shall be concerned entirely with collision broadening, i.e., the broadening of spectral lines due to collisions of the radiating atom(s) with perturbing particles. For our discussion we will restrict the perturbing particle to a neutral atom, different in species from the radiating atom, though many of the following results are applicable to broadening by other types of perturbers. The field of broadening by neutral nonresonant collisions has recently been reviewed by Allard and Kielkopf.[17] For a more complete discussion the reader is referred to this review and references therein.

A discussion of line broadening is pertinent to the problem of redistribution because the essential physics in each is really the same. Figure 1(a) is a schematic of a redistribution scattering experiment. Light of frequency ω_L is incident on an atomic system, initially in its ground state, undergoing collisions with perturbers. (If the lower state is an excited state, the scattering is quantitatively different.) The incident light will be redistributed in frequency to give an observed spectrum different from the incident spectrum, see Fig. 1(b). A typical absorption line-broadening experiment would send white light upon the same system and observe the spectrum of the transmitted light. Clearly the two experiments are similar since any light redistributed in frequency (fluorescence peak) or redistributed in propagation directly (Rayleigh peak) will show up as a loss in transmitted light. Both line broadening and redistribution depend on the physics of the collision between radiator and perturber.

We want to describe the physical origin of the different regions of line shapes. To do this we adopt the classical model of a radiating atom as being an oscillating dipole. The dipole produces an electric field $E(t)$ whose Fourier transform gives the frequency space amplitude

$$E(\omega)=\frac{1}{\sqrt{2\pi}}\lim_{T\to\infty}\int_{-T/2}^{T/2}E(t)e^{i\omega t}dt\ . \tag{1}$$

The observed intensity distribution will be proportional to the square of the frequency amplitude,

$$I(\omega)\propto\lim_{T\to\infty}\left[\frac{1}{T}\,|E(\omega)|^2\right]. \tag{2}$$

The radiating atom is assumed to be radiating very near its natural frequency of ω_0. This means we may write $E(t)=E_1(t)e^{-i\omega_0 t}$ where $E_1(t)$ is the time variation of the amplitude due to collisions. Rewriting the frequency amplitude we have

$$E(\omega)=\frac{1}{\sqrt{2\pi}}\lim_{T\to\infty}\int_{-T/2}^{T/2}E_1(t)e^{i\Delta\omega t}dt\ , \tag{3}$$

where $\Delta\omega\equiv\omega-\omega_0$ is the detuning from the resonant frequency. The only way $E(\omega)$ can be appreciable at a given ω is if $E_1(t)$ has oscillations at $\sim\Delta\omega$. In other words we need oscillations in $E_1(t)$ on the time scale of t_i,

$$t_i=\frac{1}{\Delta\omega}\ , \tag{4}$$

where t_i is called the "time of interest" for producing light at a detuning $\Delta\omega$.

Having established the time scale important for the spectrum, we now define the proper time scales for the radiating atom undergoing collisions. Our radiating atom is represented by an oscillating $E(t)$. The effect of collisions is to change the frequency of the oscillations during the collisions,[18] as shown in Fig. 2. From Fig. 2 we see that τ_c is the duration of a single collision ($\sim$1 picosecond for neutral collisions) and T_c is the time between collisions. We have implicitly made the binary-collision approximation, which presumes that strong collisions (collisions strong enough to appreciably change the frequency of the oscillating dipole) are well separated in time, i.e., $T_c\gg\tau_c$. For neutral collisions, e.g., Ba-Ar, the binary-collision approximation breaks down at a perturber pressure of ap-

proximately 28 atm. The two major regions of line profiles can be understood in terms of the two times τ_c and t_i.

1. Impact region

The impact region of the line profile is the region where $t_i \gg \tau_c$. In terms of detuning, this is given by

$$\Delta\omega \ll \tau_c^{-1} . \tag{5}$$

Since the time of interest is large compared to the collision duration, it is only the integrated effect of a collision that is important. A theory based on the model discussed above and which integrates the phase shifts caused by collisions was developed by Lindholm.[19] He found the line shape was described by a Lorentzian profile:

$$I(\omega) \propto \frac{\gamma_c}{\pi} \frac{1}{(\Delta\omega-\delta)^2+\gamma_c^2} . \tag{6}$$

The Lorentzian is shifted from the natural frequency ω_0 by δ and has a half-width at half-maximum (HWHM) given by γ_c. We will normally be concerned with detunings large compared to the shift (typically $\delta \sim \gamma_c$). The width (and shift) depends on the interaction between radiator and perturber. The long-range van der Waals interaction ($V=-C_6R^{-6}$) will be of interest to us below, and so we give the result for the width,[20]

$$\gamma_c = 4.04 N_p C_6^{2/5} \bar{v}^{3/5} , \tag{7}$$

where $\bar{v}$ is the average relative velocity and N_p is the density of perturbers.

All of the data to be presented later is for detunings outside the impact region. It is important, though, to recognize that as we approach the impact region at small detunings, the physics of the broadening (and redistribution) is different from that of the quasistatic region to be discussed in Sec. II A 2.

2. Quasistatic region

The quasistatic region of the line profile is determined by $t_i \ll \tau_c$; or in terms of detuning,

$$\Delta\omega \gg \tau_c^{-1} . \tag{8}$$

The time of interest being much less than the collision time means that details of the collision are important in determining far-wing emission or absorption. In particular, we expect the adiabatic interatomic potential curves (which govern the details of thermal-energy collisions) to play an important role. Far-wing emission or absorption can therefore be thought of as a probe of transient diatomic collision complexes.

Quasistatic theory is an application of the Franck-Condon principle which states that transitions in molecules occur at a definite internuclear separation (nuclear motion slow compared to electronic motion). Figure 3 shows hypothetical interatomic potentials for atom A and perturber $\mathscr{P}$. Quasistatic theory says the transition between ground and excited states occurs at the internuclear separation(s), called the Condon point(s), where the photon energy (emitted or absorbed) is equal to the difference between the potential curves,

$$\hbar\omega = V_e(R_c(\omega)) - V_g(R_c(\omega)) \equiv \Delta V(R_c(\omega)) . \tag{9}$$

A straightforward application of these ideas leads to the following absorption line shape:[2]

$$I_{\text{abs}}(\omega) \propto \frac{4\pi R_c^2(\omega)}{\left|\frac{d(\Delta V)}{dR}\right|_{R_c(\omega)}} \exp\left[-\frac{V_g(R_c(\omega))}{kT}\right] . \tag{10}$$

(Here we have assumed that any bound states in a ground-state potential well are in thermal equilibrium with the continuum states.) The difference between the impact and quasistatic regions is now apparent: The quasistatic region probes localized parts of the potential, while the impact region probes the nonlocalized, integrated effect of the collision.

From expression (10) it is clear that the line shape contains information about the potential curves, as expected. This has been used in circumstances where only one excited-state potential is accessible to determine ground- and excited-state potentials by measuring the line shape as a function of temperature. Such temperature-dependent line-shape experiments have been carried out for alkali-metal—rare-gas systems[21] and also for Hg-Ar, Hg-Kr, Hg-Xe,[22] two-electron systems similar to Ba—rare-gas systems.

Temperature-dependent experiments are somewhat difficult and are not very common. More common are line-shape experiments for a single temperature. Analysis of a

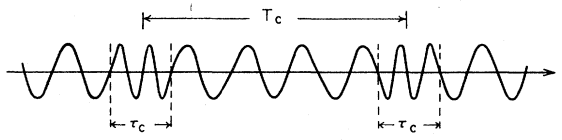

FIG. 2. Electric field of an oscillating dipole undergoing collisions. The duration of a collision and the time between collisions are τ_c and T_c, respectively.

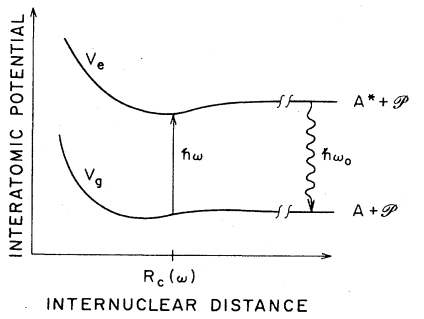

FIG. 3. Hypothetical interatomic potentials between atom A and perturber $\mathscr{P}$. A^* denotes atom A in an excited state. $R_c(\omega)$ is called the Condon point.

single temperature line shape usually involves dropping the exponential in (10) (weak ground-state interaction with perturber) and assuming a functional form of $\Delta V(R)$, such as a van der Waals or Lennard-Jones $(-C_6R^{-6}+C_{12}R^{-12})$ interaction. The quasistatic red-wing line shape predicted for a van der Waals interaction has a particularly simple form,

$$I(\omega)\propto\frac{C_6^{1/2}}{(\Delta\omega)^{3/2}}\ , \tag{11}$$

that is noticeably different from the impact-region Lorentzian.

The separation of the line profile into the impact and quasistatic regions is largely a matter of convenience. The intermediate region where $\Delta\omega\sim\tau_c^{-1}$ does not lend itself to simple physical interpretations like those above for the impact and quasistatic regions. Line-broadening theories are capable of giving a unified description of the line profile[23,24] but will not be discussed.

3. *Antistatic region*

The impact and quasistatic regions of the line profile are the most commonly encountered. For some systems though, regions are encountered where Eq. (9) cannot be satisfied for real $R_c(\omega)$. That is, the region is at detunings large enough to be quasistatic but there is no excited-state potential to which one can excite. Regions of this type are called antistatic and have been discussed by Szudy and Baylis[23] and more recently by Walkup.[25] The line-shape formula for this region is similar to the quasistatic expression but is multiplied by an exponential damping factor. The general line-shape function is not important for our purposes but we would like to give an expression for a van der Waals potential,[23,25]

$$I(\Delta\omega)\propto\frac{C_6^{1/2}}{|\Delta\omega|^{3/2}}\exp(-aC_6^{1/9}|\Delta\omega|^{5/9})\ , \tag{12}$$

where a is a constant depending on the relative velocity of atom and perturber. A van der Waals potential is attractive, so one expects Eq. (12) to hold for the blue wing at detunings large compared to τ_c^{-1}.

4. *Satellite region*

The last feature of line shapes we wish to briefly discuss occurs in the quasistatic wing and is associated with an extremum in the difference potential, i.e., $d(\Delta V)/dR=0$. According to Eq. (10) a singularity is encountered when $d(\Delta V)/dR=0$. This is only because the approximations used to obtain Eq. (10) are too crude in this region. A proper quantal or semiclassical treatment, such as that of Sando and Wormhoudt[26] or Bieniek and Streeter,[27] removes the singularity but still gives rise to enhancement of the line profile. This structure is called a satellite and often appears in far-wing spectra. Figure 4 illustrates what happens at a satellite. As we increase the detuning and approach the potential minimum of the well, the two Condon points (the two internuclear separations of excitation) approach each other and eventually coalesce. The depth $\Delta\omega_s$ of the difference-potential minimum of the well is found to correspond (see Refs. 26 or 27) to the detuning at a point beyond the satellite where the intensity is roughly 65% of the peak satellite intensity. Beyond the well-depth detuning $\Delta\omega_s$ we have no potential to excite to and the line shape becomes antistatic, and therefore drops off exponentially:[26]

$$I(\Delta\omega>\Delta\omega_s)\propto\frac{[\Delta V''(R_s)]^{1/6}}{|\Delta\omega_s-\Delta\omega|^{1/2}}\times\exp\left[-b\frac{|\Delta\omega_s-\Delta\omega|}{[\Delta V''(R_s)]^{1/3}}\right], \tag{13}$$

where b is a constant depending on temperature and $\Delta V''(R_s)$ is the second derivative of $\Delta V(R)$ evaluated at R_s, the well location. So in addition to the well depth obtained by the satellite position (65% rule), the second derivative of the difference potential at R_s can be obtained from the rate of exponential decay. This makes satellite analysis a useful tool in determining interatomic potentials.[28]

There are other interesting phenomena (e.g., quantum oscillations) in the field of line shapes which we shall not discuss. We refer the reader to Allard and Kielkopf[17] and references therein.

B. Depolarization

The measured polarization of the emitted fluorescence is the combined outcome of three processes: (i) initial alignment determined by the collision in which the excitation takes place, (ii) during the lifetime of the excited state depolarization is caused by subsequent collisions with perturber atoms, and (iii) hyperfine interactions for isotopes

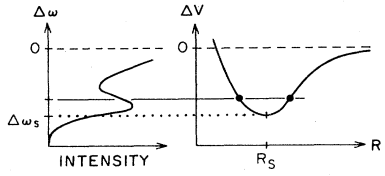

FIG. 4. Satellite resulting from a minimum in the difference potential. R_s is the internuclear separation of the difference potential minimum. $\Delta\omega_s\cdot\hbar$ is the depth of the well.

with nonzero nuclear spin. Since, as will be detailed below, it is the initial alignment which contains the useful information about the collision dynamics of the quasimolecule, the zero-pressure polarization is retrieved by measuring the pressure dependence of the polarization of the fluorescence radiation. This zero-pressure polarization is subsequently corrected for hfs effects.

1. Pressure dependence

According to the theory of Burnett and Cooper[11] the pressure dependence of the quantity β,[29,30] related to the measured polarization P_M, is given by

$$\frac{1}{\beta}=\frac{3-P_M}{2P_M}=\frac{1}{\alpha_M^{(2)}(\omega_L)}\left[1+\frac{1}{\gamma_N}\frac{\gamma_c^{(2)}}{N_p}N_p\right]. \tag{14}$$

Here $\tau_N=1/\gamma_N=8.37$ ns is the lifetime of the Ba 6^1P level, $\gamma_c^{(2)}/N_p$ is the alignment decay rate, and N_p is the perturber density. The measured parameter $\alpha_M^{(2)}(\omega_L)$ depends on laser frequency and is related to the generalized line profile $f^{(2)}(\omega_L)$.[3,12] Equation (14) predicts a linear dependence of $(3-P_M)/2P_M$ with rare-gas pressure. The slope of this line is seen to depend on ω_L, while the intercept with the pressure axis [with the second factor $(\cdots)=0$] does not. Figure 5 shows an example of such a measurement for Ba-Ar at a detuning $\Delta\omega=-4.4$ cm^{-1} and a temperature of 900 K. Having determined $\gamma_c^{(2)}/N_p$, the zero-pressure polarizations are easily evaluated from polarizations measured at a finite pressure.

2. Effects of hyperfine structure

Eighty-two percent of the atoms of naturally abundant barium have zero nuclear spin while 18% have $I=\frac{3}{2}$ (^{135}Ba, ^{137}Ba). The size of the hyperfine interaction is such (see Baird *et al.*[31]) that the hyperfine structure has time to develop almost fully before decay ($\Delta\omega_{\rm hfs}\tau_N\gg1$), while, on the other hand, it does not play a role *during* the collision ($\Delta\omega_{\rm hfs}\tau_c\ll1$). In terms of the usual sublevel populations $\sigma_{|M_L|}$, the polarization of a ^1S-^1P transition is $P=(\sigma_0-\sigma_1)/(\sigma_0+\sigma_1)$ for $I=0$, while $P=111(\sigma_0-\sigma_1)/(337\sigma_0+563\sigma_1)$ for $I=\frac{3}{2}$.[32] Denoting by q the fraction of $I=\frac{3}{2}$ atoms, we thus get the following relation:

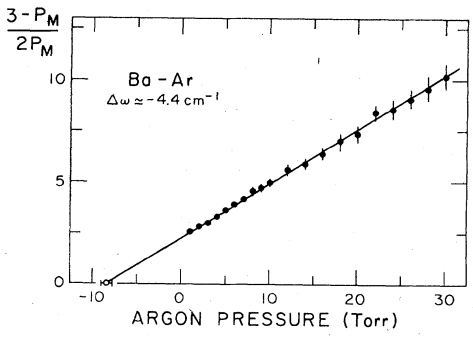

FIG. 5. Pressure dependence of the quantity $1/\beta$ is illustrated for the Ba-Ar system at $\Delta\omega=-4.4$ cm^{-1}. Compare with Eq. (14).

$$P=P_0/[1-q\tfrac{113}{450}(3-P_0)] \tag{15}$$

between the actual (zero-pressure) polarization P_0 and the polarization P obtained if no hfs effects were present. Since $q=0.18$ this reduction is significant and may amount to a 13% correction. The zero-pressure polarizations have therefore been hfs corrected according to Eq. (15).[33]

It is noteworthy that the presence of hfs does not affect the $\gamma_c^{(2)}/N_p$ determination described in Sec. II B 1: The common intercept with the pressure axis is unchanged, while the slope is increased according to

$$\alpha_M^{(2)}=\alpha^{(2)}(1-\tfrac{113}{150}q),$$

where $\alpha^{(2)}$ is the value in the absence of hfs.

3. Collision-induced alignment

We will now discuss the collision physics responsible for the alignment accompanying the production of an excited state. In the impact region defined above, where the scattering experiment only probes an overall property of the atom-perturber interaction, the polarization is given by[34]

$$P=\frac{6(\gamma_c/\gamma_c^{(2)})-3}{6(\gamma_c/\gamma_c^{(2)})-1} \tag{16}$$

and thus adds no further information to what can be learned from a line-shape measurement (γ_c) and the pressure dependence ($\gamma_c^{(2)}$).

However, in the quasistatic region where the excitation takes place between interatomic potential curves with well-defined quantum numbers Λ (angular-momentum projection along internuclear axis) at a well-localized distance (see Fig. 3), the situation is very different. A rigorous analysis may be found elsewhere,[3,4,13,35] so here we shall only outline the essential qualitative aspects and emphasize which quasimolecular parameters control the resulting polarization.

For the systems of interest here, the incoming channel is $^1S+^1S$, giving rise to a Σ potential curve, while the outgoing channel may have either Σ or Π symmetry, corresponding to the $^1P+^1S$ asymptotic states. Consider first the following case.

$\Sigma\rightarrow\Sigma$ *excitation:* Figure 6(a) shows schematically the collision plane with the Ba atom, initially in its ground state, moving along a straight-line trajectory. At the Condon point R_c, the quasimolecule may be transferred from its ground state to the excited Σ state, which has the usual shape of a p orbital oriented along the internuclear axis, as shown. At short distances, where the Ba—rare-gas interaction is strong, the orientation of the orbital is locked to the internuclear axis and thus undergoes a rotation of an angle ϕ from the point of excitation (*i*) to a point (*ii*) further along the trajectory where the interaction gets so weak that the motion of the orbital is decoupled from the internuclear axis from then on. This decoupling radius $R_{\rm dec}$ is related to the distance where the energy difference between the two merging Σ and Π potential curves is comparable to the coupling caused by the rotation of the internuclear axis.[36–39] $R_{\rm dec}$ is, for convenience, assumed

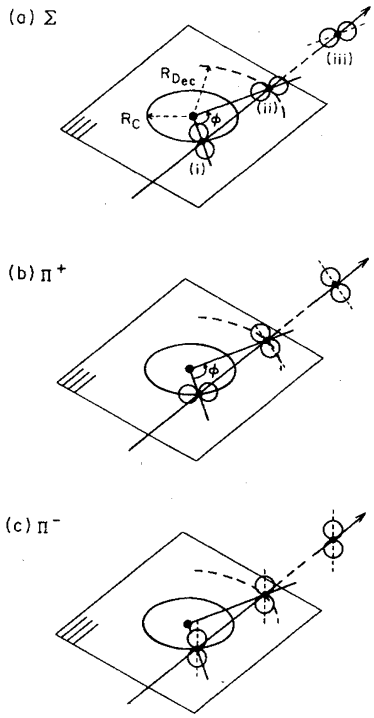

FIG. 6. This graph illustrates qualitatively the time evolution of the orientation of the excited-state orbital from (*i*) the point of excitation at a radius R_c to (*ii*) the point of decoupling at a radius R_{dec}, for the three cases of excitation of (a) the Σ state, (b) the Π^+ state, and (c) the Π^- state. The optical decay takes place at the point (*iii*). For further discussion see the text.

independent of the impact parameter and point of excitation along the trajectory, and thus independent of detuning. We also assume that $R_{dec} \geq R_c$. From the point (*ii*) the orbital is assumed to stay fixed in space without change of shape until the radiative decay at point (*iii*).

Assuming straight-line trajectories and an excitation probability amplitude proportional to the component of the electric vector along the internuclear axis, one gets by averaging over all impact parameters and all orientations of the collision plane with respect to the direction of the (linear) laser polarization, the following fluorescence polarization:

$$P_{\Sigma} = \frac{9x^2}{25+3x^2} , \tag{17}$$

where $x = R_c/R_{dec}$. The polarization is thus a maximum $\frac{9}{28} \simeq 32\%$ at $R_c = R_{dec}$, and decreases to 0% in the limit where $R_c \ll R_{dec}$. We note, however, that for a very small excitation radius, corresponding to large detunings $|\Delta\omega|$, the assumption of a straight-line trajectory breaks down, since the trajectory now passes a region where the potential curves are strongly repulsive. This will bend the trajectory and *reduce* the rotation angle ϕ, corresponding to an *increase* in the resulting polarization. The size of the trajectory effect was estimated by Lewis *et al.*[4] Using a simple hard-sphere model they obtained a polarization of ~33% for Σ-Σ excitation at the large detuning limit.

Σ→Π *excitation:* The discussion of polarization resulting from a Σ→Π transition follows the same lines, but the quantitative result is different, since a Π orbital may be decomposed in two components, Π^+ and Π^-, where the index refers to the reflection symmetry with respect to the scattering plane. Consider first the excitation of a Π^+ orbital, Fig. 6(b). Apart from the initial rotation of 90° in the scattering plane, the reorientation of the orbital during the collision is the same as that encountered in the Σ-Σ case above, so the depolarizing influence is the same for the same excitation radius. However, a Π^- orbital, oriented perpendicular to the scattering plane, keeps its orientation in space during the whole period from creation to decay, and thus suffers no depolarization at all. Under the same assumptions as above, (17) is replaced by

$$P_{\Pi} = \frac{15+15x+9x^2}{55+5x+3x^2} . \tag{18}$$

In this case the maximum polarization is $\frac{13}{21} \simeq 62\%$ ($R_c = R_{dec}$), while the minimum polarization is $\frac{3}{11} \simeq 27\%$ ($R_c \ll R_{dec}$). For the same reasons as above, trajectory effects at large detunings $|\Delta\omega|$ will increase the polarization to a value larger than the straight-line trajectory result. The hard-sphere model estimate of the polarization for Σ→Π excitation is ~56% at large detunings.[4]

To summarize the analysis, we see that for both Σ and Π excitation the polarization will decrease with decreasing excitation radius as long as the trajectories are straight. For the same excitation radius Σ excitation will yield a smaller polarization than Π excitation since the Π component perpendicular to the scattering plane is not rotated. Σ excitation may in the large detuning limit result in 0% polarization, while pure Π excitation will never result in a polarization smaller than 27%. Trajectory effects at large detunings will tend to *increase* the polarization.

The theoretical analysis of Grosser[38] supports the assumption, at least for cross-section results, of a decoupling radius being independent of impact parameter and detuning for an inverse power potential ($V \propto R^{-n}$, $n \geq 3$), where Σ and Π states rapidly separate as R becomes small. However, he also finds that due to mixing between the various states, the orbital may change shape after the point of excitation: Starting from a pure Σ or Π^+ orbital, considerable *circular* polarization may develop with increasing impact parameter. In our geometry the integrated effect of circular polarization will average to zero, but this effect will tend to *decrease* the resulting *linear* polarization of the integrated emission, and may have substantial effect since the large impact parameters are weighted heavily in the integrated emission.

The above discussion has been restricted to a single Condon point. In general, depending on the shape of the potential curves, several Condon points may occur for a given detuning $\Delta\omega$. The resulting polarization then has to be calculated by proper weighting of the individual contributions. For the present purpose, however, the observations above are sufficient.

III. EXPERIMENT

A. Experimental setup and procedure

We have performed a redistribution scattering experiment similar to that illustrated in Fig. 1(a). Such experi-

ments have been done previously for strontium being perturbed by rare-gas atoms.[16] In the strontium experiment the polarization of the emitted fluorescence was measured as a function of detuning. We have made the same polarization measurement for barium being perturbed by argon and xenon. In addition, we have also measured the redistribution coefficient (defined below) as a function of detuning.

The experimental setup is shown in Fig. 7. It is very similar to the one used in the strontium experiment.[40] An argon-ion laser at 5145 Å pumps a Coherent 590 dye laser using Rhodamine 560 laser dye. The dye laser is tuned near the Ba resonance line of 5535 Å ($J=0\rightarrow J=1$ transition) and has a full width of ~ 1 cm^{-1}. The vertically polarized dye-laser output is rotated 90° by a half-wave plate ($\lambda/2$) and then sent through a double prism arrangement. The purpose of the prisms is to remove the small amount of fluorescence emitted by the dye which is on resonance with the Ba transition. Without prisms this background fluorescence was a problem for detunings greater than 200 cm^{-1}. After monitoring the wavelength (Ref. mono.) and power (power meter) of the laser, the laser is sent through a Pockels cells (Cleveland Crystal No. TX2650). The Pockels cell rotates the polarization direction of the laser by either 0° or 90° depending on which signal ($I_{\parallel}$ or $I_{\perp}$) we are interested in. The laser is then chopped and focused into a cell containing Ba vapor and either Ar or Xe. The laser is chopped to give a measure of background light from the cell which is then subtracted from the signal. The cell is a stainless-steel cross which is heated in the middle and cooled at the windows. The laser passes very near (~ 150 μm) a heated sapphire window[40] placed in the center of the cell. This window allows the emitted fluorescence to exit the cell without being trapped, and therefore depolarized. Upon leaving the cell the fluorescence is sent through a vertical polarizer (analyzer) and a half-wave plate and is then focused onto the slits of a 1.0 m monochromator (McPherson No. 2051). The half-wave plate is used to maximize transmission through the monochromator which has a polarization-dependent grating reflectivity. The monochromator spectrally resolves the integrated fluorescence peak from the Rayleigh peak. The output of the monochromator is incident on a photomultiplier tube (EMI No. 9893 QB/350) whose output goes to a photon-counting system. Our fluorescence sensitivity is rather good: We send approximately 10^{17} photons per second into the cell and at any given instant we have typically less than one excited atom when exciting in the far wing. We are able to detect an excited-state density on the order of $1-10$ cm^{-3}.

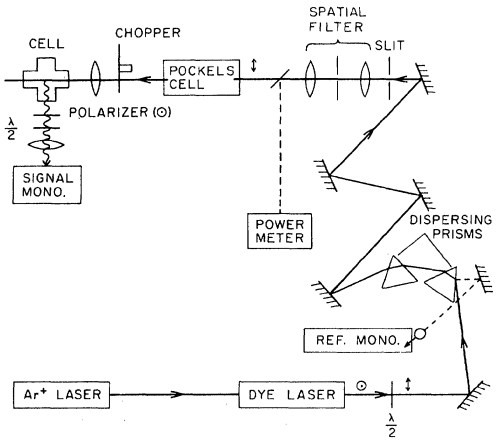

FIG. 7. Experimental setup. ⊙(↔) denotes polarization perpendicular to (in) the plane of the figure.

The polarization is measured by sending vertically polarized light into the cell to measure $I_{\parallel}$ and then sending horizontally polarized light into the cell to measure $I_{\perp}$. By changing the laser wavelength we obtain the polarization as a function of detuning. We may also calculate the quantity $I_{\parallel}+2I_{\perp}$ which is proportional to the total ^1P-state emission, i.e., the ^1P population. Referring to Fig. 3 we see that if the depth of the excited-state potential at the point of excitation is small compared to kT, the average thermal energy of the perturbers, then most atom-perturber pairs excited will dissociate and leave an excited atom. Thus, we can say every photon absorbed gives rise to an emitted fluorescent photon. If, on the other hand, the depth of the excited-state potential at the point of excitation is comparable to kT, then a fair fraction of the atom-perturber pairs excited will not have enough kinetic energy to dissociate and will therefore form bound or quasibound complexes which will radiate at wavelengths other than the resonance transition. In this case only a fraction of the absorbed photons gives rise to a fluorescent photon (frequency $\sim\omega_0$). Which of these situations exists determines whether the quantity $(I_{\parallel}+2I_{\perp})$ is proportional to the collisional absorption coefficient (the absorption coefficient due to collisions). In general the quantity describing absorption followed by emission of a fluorescent (ω_0) photon is called the redistribution coefficient. The quantity describing just the absorption during a collision is the collisional absorption coefficient. We thus use the redistribution coefficient $k_r(\Delta\omega)$ when presenting the line-shape data below.

Most of the polarization data to be presented was taken at a rare-gas pressure of 3 Torr ($\sim 3\times 10^{16}$ cm^{-3}). It is important to take the polarization data at a barium density at which the polarization is independent of barium density. If the barium density was limited only by the density at which Ba-Ba depolarizing collisions become important, then an upper limit on the Ba density would be[41] $\sim 10^{13}$ cm^{-3}. We have measured the density (see Sec. III B) at which the polarization starts decreasing with increasing density to be $\sim 10^{11}$ cm^{-3}.[42] One might think the depolarization could be due to trapping of the fluorescence, but an experiment to avoid this problem by probing the excited-state polarization with a second (tightly focused) laser suggests trapping may not be the mechanism.[43] We cannot, as yet, fully explain the depolarization that sets in at $\sim 10^{11}$ cm^{-3}, but due to this effect, we therefore took polarization data in the density range of $10^{10}-10^{11}$ cm^{-3}. This corresponded to a cell temperature of approximately 900 K, considerably higher than the vapor-pressure curve for a clean Ba surface would predict.

B. Density measurement

The physical arrangement of our cell makes it impossible to have a uniform temperature and density distribution throughout the cell. In spite of this fact one might hope to measure the coldest temperature in the vapor region of the cell and from that temperature obtain a barium density from a vapor-pressure curve. We have found this procedure to be in error by as much as 2 orders of magnitude. We have therefore chosen to measure our density by using light scattering as a probe of the density. This is by no means a new technique (see, for example, Ref. 44) for measuring number densities, but it does appear to have received very little attention by the atomic physics community. Thus we present a detailed discussion of the technique.

We use the fact that Rayleigh scattering cross sections can be quite well determined for systems such as rare gases and near the resonance transition of an atom. Knowing the cross section for Rayleigh scattering one can then measure the Rayleigh scattering from a known density of rare gas and use this measured signal to calibrate the detection system. With the detection system calibrated, a measure of the Rayleigh scattering off an unknown amount of a different gas will yield the density of that gas, if one knows its Rayleigh scattering cross section. Specifically, we use Rayleigh scattering off Xe or Ar to calibrate our detection system and then Rayleigh scattering off barium to determine the barium density.

The Rayleigh scattering process is described by the Kramers-Heisenberg equation.[45] This equation takes the following form for Rayleigh scattering off the ground state $|1\rangle$:[46]

$$\frac{d\sigma}{d\Omega}=\frac{e^4\omega^4}{\hbar^2c^4}\left|\sum_i\left[\frac{\hat{\epsilon}_s\cdot\vec{R}_{1i}\hat{\epsilon}\cdot\vec{R}_{i1}}{\omega_i-\omega}+\frac{\hat{\epsilon}\cdot\vec{R}_{1i}\hat{\epsilon}_s\cdot\vec{R}_{i1}}{\omega+\omega_i}\right]\right|^2, \tag{19}$$

where ω is the incident-light frequency, $\vec{R}=\sum_j\vec{r}_j$, $\hat{\epsilon}$ and $\hat{\epsilon}_s$ are the incident and scattered polarization directions, and the sum is over all dipole allowed excited states (including the continuum) with energy ω_i (ground state $|1\rangle$ has zero energy). We first consider Rayleigh scattering from a rare gas. We will assume we are not near a resonance transition of the rare gas. Noting that we are scattering off a ^1S ground state, Eq. (19) reduces to the following:[46]

$$\frac{d\sigma}{d\Omega}=\frac{e^4}{m^2c^4}|M_1|^2(\hat{\epsilon}\cdot\hat{\epsilon}_s)^2, \tag{20}$$

where

$$M_1=\frac{m\omega^2}{\hbar}\sum_i\frac{2\omega_i|X_{1i}|^2}{\omega_i^2-\omega^2}. \tag{21}$$

Relating the matrix element to the absorption f value we obtain

$$\frac{d\sigma}{d\Omega}=\alpha^2(\omega)k^4(\hat{\epsilon}\cdot\hat{\epsilon}_s)^2, \tag{22}$$

where $k=2\pi/\lambda$ and $\alpha(\omega)$ is the frequency-dependent polarizability of the rare gas

$$\alpha(\omega)=\frac{e^2}{m}\sum_i\frac{f_{1i}}{\omega_i^2-\omega^2}. \tag{23}$$

We choose the coordinate system shown in Fig. 8 for describing the scattering. The incident light propagates parallel to the z axis and is polarized parallel to the x axis. The scattered light propagates in a direction $\hat{k}_s$ specified by the usual polar angles θ and ϕ. There are two independent polarization directions for the scattered light. We choose the directions perpendicular and parallel to the scattering plane to describe the scattered polarization. With this choice of geometry Eq. (22) reduces to

$$\frac{d\sigma(\theta,\phi)}{d\Omega}=\alpha^2(\omega)k^4\times\begin{cases}\sin^2\phi\\ \cos^2\theta\cos^2\phi\end{cases}, \tag{24}$$

where $\sin^2\phi$ ($\cos^2\theta\cos^2\phi$) is for polarization perpendicular (parallel) to the scattering plane.

The polarizability can be easily estimated for frequencies less than the first resonance frequency of the rare gas. Dalgarno and Kingston[47] have given equations that estimate the polarizability to better than 1% in the visible and near uv. We have found the following expression also estimates the polarizability to better than 1% in the visible:

$$\alpha(\omega)=\alpha(0)\left[1+\left[\frac{\omega}{\omega_B}\right]^2\right], \tag{25}$$

where $\hbar\omega_B$ is the ionization energy of the rare gas and $\alpha(0)$ is the static polarizability. The static polarizabilities and ionization energies are summarized in Table I for the rare gases.[48,49] It is apparent that the heavy rare gases give rise to the largest scattered signal. One can get an estimate for the magnitude of the scattered light from the following: With a 50 mW green laser beam focused to $\sim$100-μm diam and a Xe pressure of 1 atm one can see the Rayleigh scattering with the naked eye in a darkened room.

A description of the Rayleigh scattering off an atom near resonance is also given by Eq. (19),

$$\frac{d\sigma}{d\Omega}=\frac{e^4\omega^4}{\hbar^2c^4}\frac{|\hat{\epsilon}_s\cdot\vec{R}_{1i}\hat{\epsilon}\cdot\vec{R}_{i1}|^2}{|\Delta\omega|^2}. \tag{26}$$

We have assumed that one state dominates the scattering

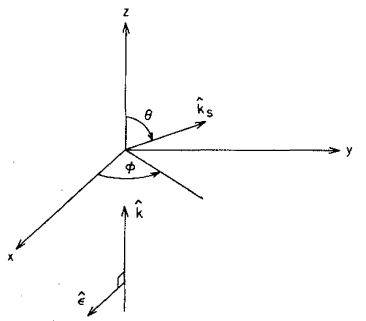

FIG. 8. Geometry for description of Rayleigh scattering.

and that the detuning from this state is large compared to the width of the line. In general this cross section is a function of dipole matrix elements which are normally available.[50] The angular dependence will depend on the system under study. For example, a $J=\frac{1}{2}\rightarrow J=\frac{1}{2}$ transition gives rise to isotropic Rayleigh scattering, while a $J=0\rightarrow J=1$ transition has the angular dependence of a classical dipole, Eq. (24). For our situation of barium ($J=0\rightarrow J=1$) we have taken $\theta=90°$ and $\phi=90°$ and we obtain

$$\frac{d\sigma(90°,90°)}{d\Omega}=\frac{1}{4}\frac{e^4}{m^2c^4}f_{12}^2\frac{\omega^2}{(\Delta\omega)^2}\times\begin{cases}1\\0\end{cases}. \tag{27}$$

The f value for the barium resonance line at 5535 Å is 1.59.[51]

The barium density is measured by first using Eq. (22) and a measurement of the Rayleigh signal off Xe (or Ar) to determine our system detection efficiency. We used the static polarizability so we have an inherent error of ~6%. [The experimental error was typically (10—50)% due to stray light in our setup. We had a fairly large amount of stray light from the laser because of our passing the laser very close (~150 μm) to a sapphire window. A correction for this stray light was also sometimes necessary in the polarization and line-shape data of the far wing due to the finite rejection (10^{-5}) of the monochromator, i.e., 10^{-5} of the stray light may be comparable to the fluorescence at large detunings.] Once the detection efficiency was determined, the Rayleigh scattering off barium at detunings of ~6 cm^{-1} was measured. Using Eq. (27) we are then able to calculate our barium density to an accuracy of typically 25%.

C. Data

1. Line shapes

The redistribution coefficient $k_r(\Delta\omega)$, per barium and perturber atom, multiplied by $(\Delta\omega)^2$ is plotted in Figs. 9 and 10 for Ba-Ar and Ba-Xe, respectively. The multiplication by $(\Delta\omega)^2$ serves to better display satellite structures. $k_r(\Delta\omega)(\Delta\omega)^2$ is proportional to $\gamma_c(\Delta\omega)$, the frequency-dependent collision rate,[12] so in these coordinates a Lorentzian line shape will yield a horizontal curve. The scatter of the points reflects the relative experimental uncertainties, while the absolute scale, established by the method described in Sec. III B, is reliable within 25%.

TABLE I. Static polarizabilities and ionization energies for the rare gases.

Gas	$\alpha(0)$ (Å^3)[a]	$\hbar\omega_B$ (eV)[b]
He	0.2050	24.59
Ne	0.3946	21.56
Ar	1.642	15.76
Kr	2.480	14.00
Xe	4.044	12.13

[a]Reference 48.
[b]Reference 49.

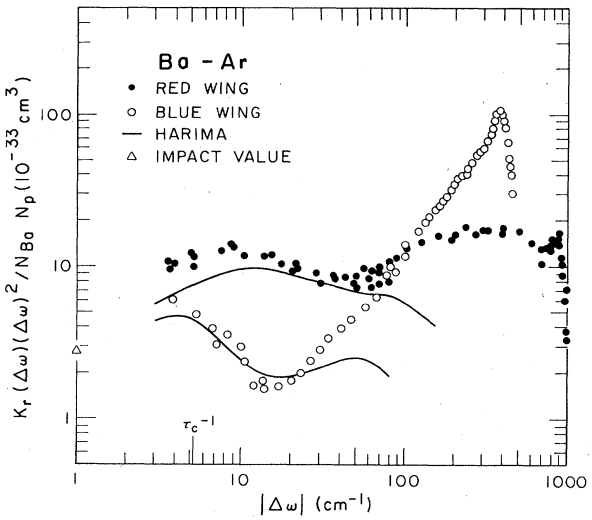

FIG. 9. Collisional redistribution coefficient $k_r(\Delta\omega)$ multiplied by $(\Delta\omega)^2$ vs detuning $\Delta\omega$ for the Ba-Ar system. ●, red wing; ○, blue wing. The solid curves are taken from Ref. 52. Note $\Delta\omega$ is short for the quantity $\Delta\omega/2\pi c$.

The solid curves are derived from absolute absorption profiles measured by Harima *et al.*[52] by an absorption technique with a claimed uncertainty of 10% in the 10—100-cm^{-1} range, 30% below 10 cm^{-1} and 60% above 100 cm^{-1}. Their method actually measures the combined absorption due to Rayleigh scattering and collisional absorption, but their experimental conditions (high rare-gas pressure) are such that the latter component dominates. For detunings small compared to kT ($kT\sim600$ cm^{-1}) where we do not create a significant number of bound states (assuming a shallow ground-state well; see Sec. IV B), the absorption coefficient and the redistribution coefficient will be equal. In most of the detuning range their data agree with the present results with respect to both the shape and the absolute size, within the combined

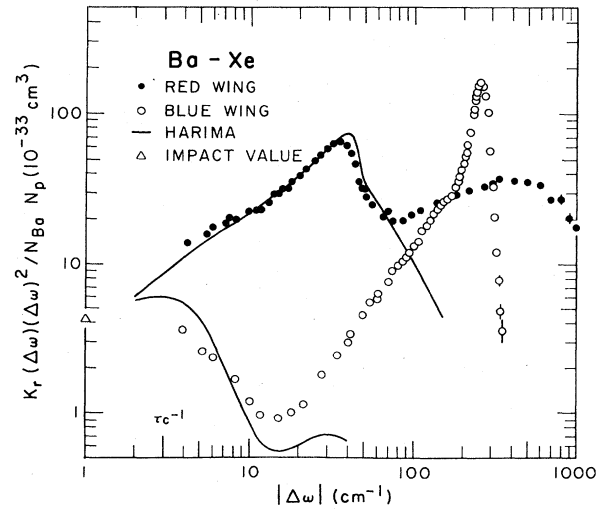

FIG. 10. Same as Fig. 9, but for Ba-Xe.

error bars. However, at the largest detunings considerable disagreement develops, with the result of Harima *et al.*[52] being much lower than our curves. The origin of this disagreement is not clear, but we suspect that it could be connected with the difficulty of detecting the very small relative change in the absorption signal at large detuning. Contrary to this, the present experiment, which instead monitors the scattered light and therefore has a much higher sensitivity as pointed out in Sec. III A, is able to determine $k_r(\Delta\omega)$ over a much larger dynamic range.

Red-wing absorption profiles have been measured by Zhuvikin *et al.*[53] Their results are also similar to those reported here but cover only the narrow range of 3—30 cm^{-1}, so we omit further discussion. For comparison we may use the results of Zhuvikin *et al.*[53] and Penkin and Shabanova[54] to obtain long-range van der Waals C_6 coefficients: For Ar, 1.42×10^{-58} erg cm^6; for Xe, 3.58×10^{-58} erg cm^6. Using these coefficients and Eq. (7) we predict values of the impact half-width which can be converted into absorption coefficients. These are displayed in Figs. 9 and 10.

The observed structures and the information they contain about the interatomic potential curves will be discussed in Sec. IV. Here we only notice the observation of pronounced blue-wing satellites near 350 cm^{-1} (Ar) and 250 cm^{-1} (Xe), and a red-wing satellite near -35 cm^{-1} (Xe). A weak, diffuse structure is seen in the -10 cm^{-1} region for Ar.

There is a strong similarity between the present line shapes and those measured for the similar systems Sr-Ar, Sr-Kr, and Sr-Xe ($|\Delta\omega| = 2$—200 cm^{-1})[55] and Hg-Ar, Hg-Kr, and Hg-Xe.[22] The latter are particularly interesting since they cover a large detuning region including the blue-wing satellite.

TABLE II. Alignment decay rates for Ba—rare-gas systems at a temperature of 900 K.

Gas	$\gamma_c^{(2)}/N_p$ ($\times10^{-9}$ cm^{3}s^{-1}) Sr[a]	Ba
Ar	1.58±0.19	1.30±0.08[b]
Kr	1.91±0.39	
Xe	2.00±0.31	1.42±0.09[b]

[a]Reference 16.
[b]This work.

2. *Alignment decay rates*

Table II shows alignment decay rates $\gamma_c^{(2)}/N_p$ for Ba-Ar and Ba-Xe determined from measurements of the pressure-dependent polarization for fixed $\Delta\omega$, see Sec. II B 1. The Ba rates are $\sim$20% smaller than the corresponding values for the Sr—rare-gas systems.[16]

3. *Collisional alignment*

The polarization of the fluorescence due to the initial collisional alignment, obtained as described in Sec. III B, is shown in Figs. 11 and 12 for the red and blue wings of the Ba-Ar and Ba-Xe systems, respectively. Again, the scatter of the points gives a feeling for the experimental uncertainty. We notice a general trend of decreasing polarization with increasing $|\Delta\omega|$, followed by an increase at even larger detunings. We also note a correlation between structures in the polarization and structures in the line shape (plotted below in order to facilitate comparison and the discussion in Sec. IV), especially clear for the Ba-

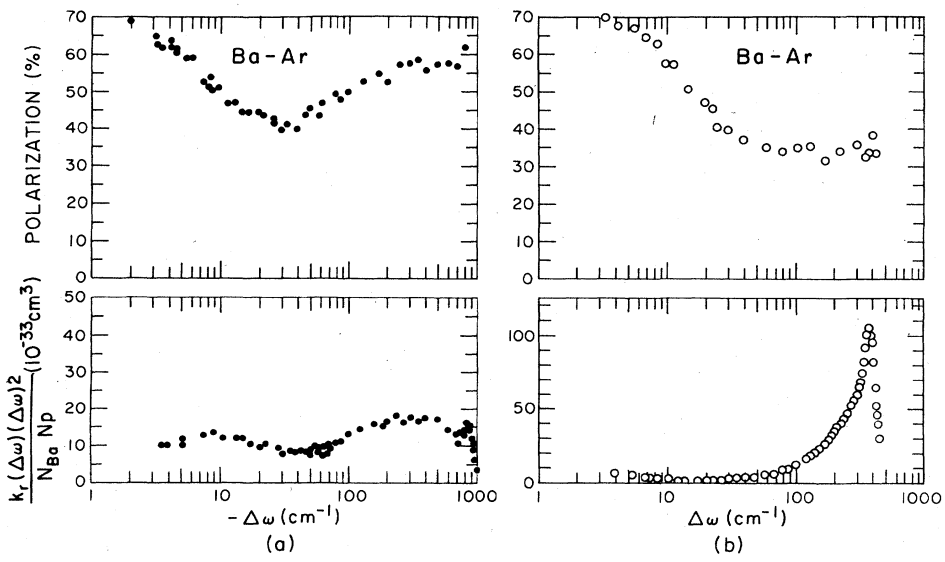

FIG. 11. Zero-pressure polarizations, corrected for hyperfine-structure effects, for the Ba-Ar (a) red and (b) blue wings. Below are plotted corresponding values of $k_r(\Delta\omega)(\Delta\omega)^2$.

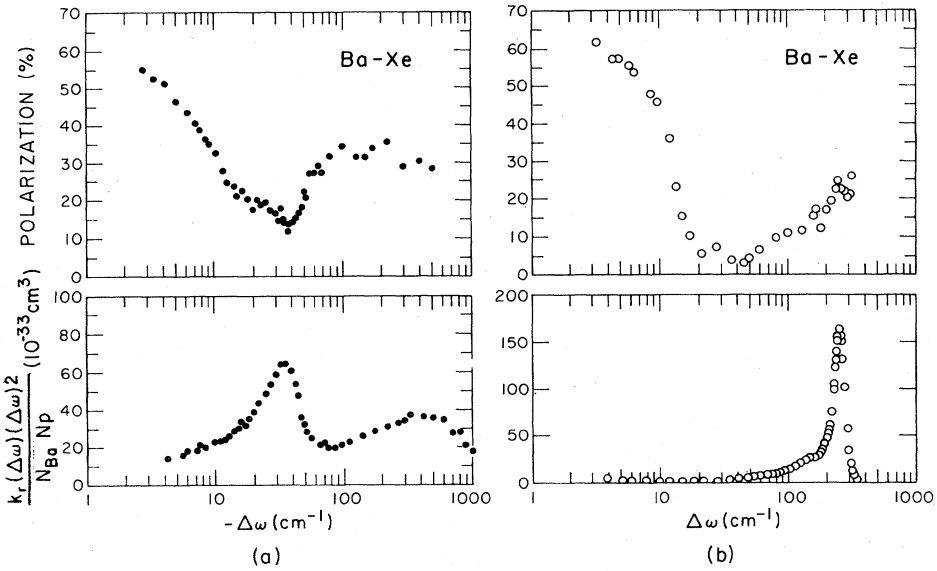

FIG. 12. Same as Fig. 10, but for Ba-Xe.

Xe red-wing satellite. The physics underlying this behavior will be displayed in Sec. IV.

As was the case for the line shapes, these results bear a strong similarity with the polarizations measured for the Sr-Ar, Sr-Kr, and Sr-Xe systems.[16]

IV. ANALYSIS

A. Line shapes and polarizations

In this section we discuss in detail the various features observed in Figs. 9—12 and in particular show how, based on the results of Sec. II, they are related to the radial dependences of the difference between the two potential curves for the two excited molecular states, $A\,^1\Sigma$ and $B\,^1\Pi$ (to be abbreviated $^*\Sigma$ and $^*\Pi$), correlating to $Ba^*(6^1P)+\mathscr{P}(^1S)$ at large internuclear separation, and the $X\,^1\Sigma$ ground-state potential (abbreviated Σ), correlating to $Ba(6^1S)+\mathscr{P}(^1S)$. The two difference curves are labeled $^*\Sigma$-Σ and $^*\Pi$-Σ, respectively, on Fig. 13(a). Also in Fig. 13 are sketches of the behavior of the red- and blue-wing line shapes (b) and polarizations (c) for the corresponding values of the detuning parameter $\Delta\omega=\omega_L-\omega_0$. The graphs are meant to be qualitative only and are believed to hold for the Ba-Ar, Kr, and Xe systems. They have the greatest resemblance to the Ba-Xe results, where several of the characteristic features are especially pronounced.

Starting with the difference potentials, Fig. 13(a), the behavior at very large internuclear distances, where only the asymptotic parts of the valence electron clouds overlap (corresponding to $\Delta\omega$ in the impact region), is governed by van der Waals potentials

$$\Delta V_{^*\Sigma\text{-}\Sigma}=-(C_{6,^*\Sigma}-C_{6,\Sigma})R^{-6}\,,$$

$$\Delta V_{^*\Pi\text{-}\Sigma}=-(C_{6,^*\Pi}-C_{6,\Sigma})R^{-6}\,.$$

Since $C_{6,^*\Sigma}>C_{6,^*\Pi}$ (Ref. 56) and $C_{6,^*\Pi}>C_{6,\Sigma}$ (Ref. 57) both difference potentials are attractive with $\Delta V_{^*\Sigma\text{-}\Sigma}$ being more attractive than $\Delta V_{^*\Pi\text{-}\Sigma}$. At shorter internuclear distances, where there is considerable overlap between the barium and rare-gas valence electron clouds, and where the corresponding detuning approaches and enters the quasistatic region, we claim the following behavior of the difference potentials: The $^*\Sigma$-Σ difference potential curve exhibits a minimum and then rises to another extremum

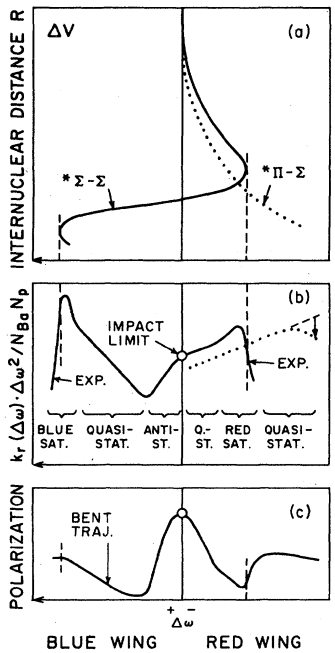

FIG. 13. Qualitative sketch of (a) the excited-state—ground-state potential difference curves vs internuclear distance, (b) the corresponding blue- and red-wing profiles (compare Figs. 9 and 10), and (c) polarizations (compare Figs. 11 and 12). Exponential satellite tails are denoted by EXP.

(>0) at a smaller internuclear distance. Contrary to this, the $^*\Pi$-Σ difference decreases monotonically in the whole internuclear range of relevance to the present results. These conclusions follow unambiguously from a combined analysis of the line shape and polarization behaviors, which we now present.

1. Impact-region limit

The borderline between the impact region and the quasistatic region is (Sec. II) given by $\Delta\omega = 1/\tau_c$. We estimate the collision time τ_c as being the Weisskopf radius divided by the mean relative velocity. Collisions with an impact parameter of the Weisskopf radius give an integrated phase shift of unity relative to the unperturbed phase. The Weisskopf radius was estimated using the C_6 values mentioned above.

Impact-limit results for the polarizations can be obtained from Eq. (16) using the $\gamma_c^{(2)}$ values of Table II and the impact-region γ_c values obtained from the results of Zhuvikin *et al.*[53] and Penkin and Shabanova.[54] This yields

$$P(\text{Ba-Ar}) = 68 \pm 2\% \ ,$$

$$P(\text{Ba-Xe}) = 70 \pm 2\% \ ,$$

for the impact limits of Ba-Ar and Ba-Xe, where the error bars correspond to the $\gamma_c^{(2)}$ uncertainty of Table II. The uncertainty due to the γ_c values is more difficult to assess. Our polarization data do not extend into the proper impact region, but inspection of Figs. 11 and 12 show that these polarization estimates are indeed reasonable asymptotic values for $\Delta\omega \to 0$.

2. Red-wing analysis

Starting from small detunings we first encounter a region where approximately $I(\Delta\omega) \propto |\Delta\omega|^{-3/2}$ [cf. Eq. (11)]. It is labeled quasistatic on Fig. 13(b), though $\Delta\omega$ is not sufficiently larger than $1/\tau_c$ for this label to be strictly true. In this region quasistatic excitation to the potential difference curves contribute to the line shape, and there are three Condon points, though the innermost Condon point for the $^*\Sigma$-Σ difference potential only contributes slightly. The polarization drops rapidly in this region, cf. Eqs. (17) and (18), since the important Condon points move inwards with increasing detuning. The situation changes when we approach the bottom of the $^*\Sigma$-Σ well where the corresponding Condon points will dominate the line shape due to the near-singularity of the denominator in Eq. (10) and form a red-wing satellite, cf. Sec. II A 4. The polarization here has a minimum which for Ba-Xe is so pronounced that it unambiguously labels the origin of the satellite to be a $^*\Sigma$-Σ excitation, cf. Sec. II B 3. Beyond the satellite the contribution from the $^*\Sigma$-Σ potential difference curve drops exponentially, leaving only the $^*\Pi$-Σ contribution, leading to a rise in the polarization. Beyond $\Delta\omega = 500$ cm^{-1} the line shape changes again as indicated with the arrow in Fig. 13(b). The observed decay is not exponential and the origin of this feature is not completely clear. However, a likely cause could be the $\exp\{-V_g[R(\Delta\omega)]/kT\}$ depletion [Eq. (10)] of the ground-state potential, which turns repulsive at short distances (see Sec. IV B) though the structure observed in the Ba-Ar far red wing suggests that more may be happening.

3. Blue-wing analysis

Turning now to the blue wings, we first note a fast drop of the line shape, out to about 15 cm^{-1}. This is the antistatic region of the long-range van der Waals part of the difference potential (Sec. III A 3), and displays the rapid decrease due to the exponential factor in Eq. (12). At larger detunings, quasistatic excitation to the short-range repulsive part of the $^*\Sigma$-Σ difference potential becomes dominant. In this region both the excitation radius and the slope change slowly, so $I(\Delta\omega)$ varies little, cf. Eq. (10). The polarization stays roughly constant, and the small polarization value for Ba-Xe unambiguously labels the excitation as a Σ-Σ transition. Because the excitation radius here is quite small, we expect trajectory effects may become important, and we attribute the rise seen for the Ba-Xe polarization to be due to this effect. Even further out we reach the blue-wing satellite due to the local maximum in the $^*\Sigma$-Σ difference potential. Beyond the peak the intensity drops exponentially with detuning [see Eq. (13)]. This characteristic dependence was most clearly seen for the Ba-Xe system, as illustrated in Fig. 14(a). We

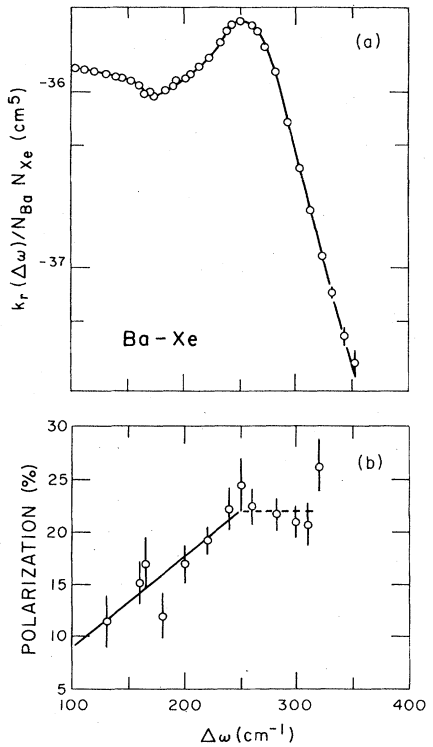

FIG. 14. Detailed study of (a) the Ba-Xe blue-wing satellite, showing the exponential decay at detunings beyond the peak; (b) shows the corresponding polarization. For a discussion see the text.

were able to follow the exponential decay for about 2 orders of magnitude in a rather small detuning range. Since in this range beyond the peak the excitation takes place in a fixed, narrow internuclear region (but the probability decreases exponentially), we expect the polarization to stay constant. As seen in Fig. 14(b) this seems indeed to be the case though the error bars do not provide conclusive evidence.

4. Decoupling radius

The equations for the polarization given in Sec. II B 3, Eqs. (17) and (18), depend solely on the ratio of the excitation radius to the decoupling radius $x=R_c/R_{\rm dec}$. Grosser[38] has given the following expression for the decoupling radius:

$$R_{\rm dec}=\left[\frac{|\Delta C_6|}{5\hbar\bar{v}}\right]^{1/5} \tag{28}$$

for a van der Waals potential. The average velocity is given by $\bar{v}$ and

$$\Delta C_6=C_6(^*\Sigma)-C_6(^*\Pi)\ .$$

From the results of Zhuvikin *et al.*[53] and Penkin and Shabanova[54] we estimate $1/\hbar\Delta C_6=2.0\times10^{-43}$ m^6/s for Ba-Xe. Substituting in Eq. (28) we obtain $R_{\rm dec}\approx6$ Å. Assuming excitation radii of 4.5 and 5.0 Å for $^*\Sigma$ and $^*\Pi$ excitation, respectively, this yields

$$P_\Sigma\sim20\%\ ,$$

$$P_\Pi\sim56\%\ .$$

This assumes straight-line trajectories, so one would expect (assuming a van der Waals potential is valid) to see these polarizations at large detunings before trajectory effects become significant, e.g., for Ba-Xe, $\Delta\omega\sim-110$ cm^{-1} for Π excitation. The observed polarization at say $\Delta\omega\sim-110$ cm^{-1} is $\sim33\%$, well below the 56% a van der Waals potential would predict using Grosser's condition, Eq. (28). We believe this is due to the fact that van der Waals $^*\Sigma$ and $^*\Pi$ potentials diverge rather rapidly at small internuclear separations, whereas the actual $^*\Sigma$ and $^*\Pi$ potentials for the Ba-Xe system are less strongly divergent at large R and even have a curve crossing at somewhat smaller R (see Sec. IV B and Fig. 15). Thus there is a larger region of R space where the $^*\Sigma$ and $^*\Pi$ states can mix. This leads, as indicated below, to more depolarization over what a van der Waals potential would predict.

The use of a definite decoupling radius is in fact only a simple way of approximating the transition from molecular eigenstates to atomic eigenstates, in order to describe the final orientation of the ^1P orbital after a collision. In addition to the reorientation that may occur during a collision, the shape of the $^*\Sigma$ and $^*\Pi^+$ orbitals can be changed if mixing occurs throughout the collision (rather than decoupling just at $R_{\rm dec}$).[38] This would give rise to more depolarization than the reorientation model would predict. Thus the reorientation model may not be quantitatively correct when the $^*\Sigma$ and $^*\Pi^+$ states interact over a large region of R to change the shape of orbitals.

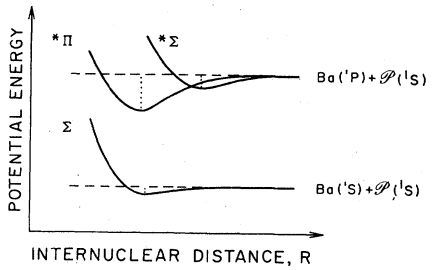

FIG. 15. Qualitative sketch of the interatomic potentials for Ba—rare-gas systems.

B. Potentials

A temperature-dependent line-shape experiment is necessary to extract interatomic potentials from line-shape data. We cannot, therefore, extract potentials from our results. We can, however, discuss the qualitative behavior the potentials must have in order to be consistent with our results and interpretation.

It is instructive to consider what is known about similar systems. Table III gives the approximate potential well depths for cesium and mercury systems. Barium has a core radius approximately halfway between cesium and mercury.[58] Thus one may expect core-core repulsion to be appreciable at an internuclear separation less than that of Cs-$\mathscr{P}$ but greater than that of Hg-$\mathscr{P}$, the perturber $\mathscr{P}$ denoting any of the rare gases. If the long-range attractive potentials are similar for the three systems (Cs-$\mathscr{P}$, Ba-$\mathscr{P}$, and Hg-$\mathscr{P}$), one would then expect the well depths to increase in going from cesium to mercury. From Table III we see the well depths certainly are larger for mercury than for cesium. So it is reasonable to expect Ba-$\mathscr{P}$ well depths will be between Cs-$\mathscr{P}$ and Hg-$\mathscr{P}$ depths. We should also note that the depths should be larger for xenon than for argon since the polarizability and therefore the van der Waals interaction is larger for xenon.

We thus expect the Ba-$\mathscr{P}$ potentials to have the form indicated in Fig. 15. The ground state has a shallow well (<200 cm^{-1}) and becomes repulsive at small internuclear separation. The excited Σ state ($^*\Sigma$) has a long-range van der Waals potential which becomes repulsive at smaller R due to the electron overlap of the ^1P orbital with the rare-gas electron cloud. The $^*\Sigma$ well depth must be less than or approximately 35 cm^{-1} (10 cm^{-1}) for Ba-Xe (Ba-Ar) given the satellite position. The Π state has a long-range van der Waals potential which crosses the $^*\Sigma$ curve. The

TABLE III. Approximate interatomic potential well depths for systems similar to Ba-Ar and Xe. Well depths are given in wave numbers (cm^{-1}).

	Σ		$^*\Sigma$		$^*\Pi$	
Perturber	Cs[a]	Hg[b]	Cs[a]	Hg[b]	Cs[a]	Hg[b]
Ar	50	140	0	40	300≥	700
Kr	60	175	0	65	350≥	1300
Xe	75	220	0	115	500≥	2000

[a]Reference 2.
[b]Reference 22.

depth of the Π-state well is probably between 300 and 2000 cm^{-1} for both Ba-Ar and Xe. The potentials in Fig. 15 should also be representative of similar two-electron systems (Mg, Ca, Sr, Zn, Cd, and Hg) being perturbed by the heavy rare gases (Ar, Kr, and Xe).

V. CONCLUDING REMARKS

The combined analysis of line shape and polarization for the Ba-Ar and Xe systems labels unambiguously the various prominent structures seen in the experimental results, and their relation to characteristic features of the excited-atom—rare-gas difference potentials, and their molecular quantum numbers. We thus believe our detailed interpretation (see Fig. 13) to be qualitatively correct, but have, on the other hand, resisted the temptation to fit the observations to a simple model potential, like a harmonic well or a Lennard-Jones potential, thereby following the philosophy of Margenau who states in his 1939 review paper:[56] "Useful as this procedure has proved to be [it] is now known to be unsuited as an accurate theoretical expression for intermolecular forces." However, we also believe that the present data allow detailed tests of any future theory for the molecular structure of these systems.

The observations have in several respects strong similarities with analogous data—in all cases less complete—for several other systems with a similar electronic structure, such as Ca, Sr, and Hg perturbed by Ar, Kr, and Xe. Our interpretation, as succinctly summarized in Fig. 13, should thus be valid for these systems as well, though the absolute numbers for satellite positions, etc., are, of course, system dependent.

ACKNOWLEDGMENTS

We wish to thank R. J. Bieniek, N. Bras, A. Gallagher, H. Harima, I. V. Hertel, and P. S. Julienne for stimulating discussions, and R. Weppner for technical assistance. One of us (N.A.) acknowledges travel support from the Danish Natural Science Research Council, and another (K.B.), support by an Alfred P. Sloan Foundation fellowship. This work was supported by National Science Foundation Grant No. PHY-82-00805 to the University of Colorado and by the Atomic Plasma Radiation Division of the National Bureau of Standards.

---

*1982-83 JILA Visiting Fellow. Permanent address: Physics Laboratory II, H. C. Ørsted Institute, DK-2100 Copenhagen, Denmark.

†Present address: Blackett Laboratory, Imperial College of Science and Technology, University of London, London, SW7 2BZ, England.

[1]A. Gallagher, Acta Phys. Pol. A **54**, 721 (1978).

[2]R. E. M. Hedges, D. L. Drummond, and A. Gallagher, Phys. Rev. A **6**, 1519 (1972).

[3]J. Cooper, in *Spectral Line Shapes, Vol. 2,* edited by K. Burnett (de Gruyter, Berlin, 1983), p. 737.

[4]E. L. Lewis, M. Harris, W. J. Alford, J. Cooper, and K. Burnett, J. Phys. B **16**, 553 (1983).

[5]J. L. Carlsten, A. Szöke, and M. G. Raymer, Phys. Rev. A **15**, 1029 (1977).

[6]K. Burnett, J. Cooper, and P. D. Kleiber, Phys. Rev. A **25**, 1345 (1982); and references contained in this paper.

[7]P. D. Kleiber, K. Burnett, and J. Cooper, Phys. Rev. Lett. **47**, 1595 (1981).

[8]A. Omont, E. W. Smith, and J. Cooper, Astrophys. J. **175**, 185 (1972); **182**, 283 (1973).

[9]D. L. Huber, Phys. Rev. **178**, 93 (1969).

[10]K. Burnett, J. Cooper, R. J. Ballagh, and E. W. Smith, Phys. Rev. A **22**, 2005 (1980); K. Burnett and J. Cooper, *ibid.* **22**, 2044 (1980).

[11]K. Burnett and J. Cooper, Phys. Rev. A **22**, 2027 (1980).

[12]J. Cooper, Astrophys. J. **228**, 339 (1979).

[13]G. Nienhuis, J. Phys. B **16**, 1 (1983).

[14]A. Corney and J. V. M. McGinley, J. Phys. B **14**, 3047 (1981).

[15]P. Thomann, K. Burnett, and J. Cooper, Phys. Rev. Lett. **45**, 1325 (1980).

[16]W. J. Alford, K, Burnett, and J. Cooper, Phys. Rev. A **27**, 1310 (1983).

[17]N. Allard and J. Kielkopf, Rev. Mod. Phys. **54**, 1103 (1982).

[18]H. A. Lorentz, Proc. Acad. Sci. Amsterdam **8**, 591 (1906).

[19]E. Lindholm, Ark. Mat. Astron. Fys. **28B**, No. 3 (1941).

[20]D. Mihalas, *Stellar Atmospheres* (Freeman, San Francisco, 1970).

[21]See, for example , Ref. 2; D. L. Drummond and A. Gallagher, J. Chem. Phys. **60**, 3426 (1974); B. Cheron, B. Scheps, and A. Gallagher, *ibid.* **65**, 326 (1976).

[22]N. Bras and C. Bousquet, J. Phys. (Paris) **40**, 945 (1979); N. Bras, Thèse de Doctorat, Université Pierre et Marie Curie, Paris, 1979; C. Bousquet, N. Bras, and Y. Madji, J. Phys. B **17**, 1831 (1984).

[23]J. Szudy and W. E. Baylis, J. Quant. Spectrosc. Radiat. Transfer **15**, 641 (1975).

[24]E. W. Smith, J. Cooper, and C. B. Vidal, Phys. Rev. **189**, 149 (1969).

[25]R. E. Walkup, Phys. Rev. A **25**, 596 (1982).

[26]K. M. Sando and J. C. Wormhoudt, Phys. Rev. A **7**, 1889 (1973).

[27]R. J. Bieniek and T. J. Streeter, Phys. Rev. A **28**, 3328 (1983).

[28]C. G. Carrington and A. Gallagher, Phys. Rev. A **10**, 1464 (1974).

[29]β is equal to (minus) the alignment parameter of Fano and Macek (Ref. 30), and $\alpha^{(2)}(\omega_L)$ thus (minus) the initial collisional alignment $A_0^{\rm col}$.

[30]U. Fano and J. H. Macek, Rev. Mod. Phys. **45**, 553 (1973).

[31]P. E. G. Baird, R. J. Brambley, K. Burnett, D. N. Stacey, D. M. Warrington, and G. K. Woodgate, Proc. R. Soc. London, Ser. A **365**, 567 (1979).

[32]I. C. Percival and M. J. Seaton, Phil. Trans. R. Soc. London, Ser. A **251**, 113 (1958).

[33]For strontium this correction turns out to be negligible. The polarization results previously published by our group for the Sr—rare-gas systems (Ref. 16) thus remain valid.

[34]This expression may be derived by taking the impact limit of Eqs. (3.12)—(3.16) of Ref. 11.

[35]E. L. Lewis, J. M. Salter, and M. Harris, J. Phys. B **14**, L173 (1981).

[36]V. N. Rebane, Opt. Spectrosc. **26**, 371 (1969).

[37]P. S. Julienne, in *Spectral Line Shapes, Vol. 2,* edited by K. Burnett (de Gruyter, Berlin, 1983), p. 769.
[38]J. Grosser, J. Phys. B **14**, 1449 (1981).
[39]A. Bähring, I. V. Hertel, E. Meyer, and H. Schmidt, Z. Phys. A **312**, 293 (1983).
[40]W. J. Alford, K. Burnett, and J. Cooper, in *Spectral Line Shapes, Vol. 2,* edited by K. Burnett (de Gruyter, Berlin, 1983), p. 805.
[41]C. G. Carrington, D. N. Stacey, and J. Cooper, J. Phys. B **6**, 417 (1973).
[42]In the Sr experiment (Ref. 16), we estimated our density to be $\sim 10^{13}$ cm^{-3} based on a vapor-pressure curve. In light of the present results it is not clear what our density was in the Sr experiment; it was probably $\sim 10^{11}$ cm^{-3}.
[43]This experiment used a second laser tuned on resonance (6131 Å) from the $6s6p\ ^1P$ state to the $6s9s\ ^1S$ state. We determined the ^1P polarization by monitoring fluorescence from the $6s9s\ ^1S$ to the $6s6p\ ^3P_1$. By changing the laser beam diameters we were unable to see a change in the density at which depolarization occurs. This preliminary result suggests that trapping (which would depend on beam diameter) may not be the source of depolarization.
[44]A. W. DeSilva and A. C. Goldenbaum, in *Methods of Experimental Physics, Vol. 9—Part A,* edited by H. R. Griem and R. H. Lovberg (Academic, New York, 1970), p. 61.
[45]H. A. Kramers and W. Heisenberg, Z. Phys. **31**, 681 (1925).
[46]R. Loudon, *The Quantum Theory of Light* (Clarendon, Oxford, 1973).
[47]A. Dalgarno and A. E. Kingstom, Proc. R. Soc. London, Ser. A **259**, 424 (1969).
[48]R. R. Teachout and R. T. Pack, Atomic Data **3**, 195 (1971).
[49]C. E. Moore, *Ionization Potentials and Ionization Limits Derived from Analyses of Optical Spectra,* Natl. Bur. Stand. Ref. Data Ser., Natl. Bur. Stand. (U.S.) Circ. No. 34 (U.S. GPO, Washington, D.C., 1970).
[50]E. U. Condon and G. H. Shortley, *The Theory of Atomic Spectra* (Cambridge University, Cambridge, 1935).
[51]B. M. Miles and W. L. Wiese, Atomic Data **1**, 1 (1969).
[52]H. Harima, K. Tachibana, and Y. Urano, J. Phys. B **15**, 3679 (1982); H. Harima, Ph.D. thesis, Kyoto Technical University, 1982.
[53]G. V. Zhuvikin, N. P. Penkin, and L. N. Shabanova, Opt. Spektrosk. **46**, 1135 (1979) [Opt. Spectrosc. (USSR) **46**, 642 (1979)].
[54]N. P. Penkin and L. N. Shabanova, Opt. Spektrosk. **25**, 795 (1968) [Opt. Spectrosc. (USSR) **25**, 446 (1968)].
[55]H. Harima, Y. Fukuzo, K. Tachibana, and Y. Urano, J. Phys. B **14**, 3069 (1981); H. Harima, T. Yanagisawa, K. Tachibana, and Y. Urano, *ibid.* **16**, 4365 (1983); J. M. Farr and W. R. Hindmarsh, *ibid.* **4**, 568 (1971).
[56]H. Margenau, Rev. Mod. Phys. **11**, 1 (1939).
[57]L. N. Shabanova, Opt. Spektrosk. **36**, 23 (1974) [Opt. Spectrosc. (USSR) **36**, 13 (1979)].
[58]N. A. Sondergaard and E. A. Mason, J. Chem. Phys. **62**, 1299 (1975).